A correction to the enhanced bottom drag parameterisation of tidal turbines

Stephan C. Kramer[a,*], Matthew D. Piggott[a,b]

[a] *Applied Modelling and Computation Group, Department of Earth Science and Engineering, Imperial College London, South Kensington Campus, London SW7 2AZ, United Kingdom*
[b] *Grantham Institute for Climate Change and the Environment, Imperial College London, United Kingdom*

Abstract

Hydrodynamic modelling is an important tool for the development of tidal stream energy projects. Many hydrodynamic models incorporate the effect of tidal turbines through an enhanced bottom drag. In this paper we show that although for coarse grid resolutions (kilometre scale) the resulting force exerted on the flow agrees well with the theoretical value, the force starts decreasing with decreasing grid sizes when these become smaller than the length scale of the wake recovery. This is because the assumption that the upstream velocity can be approximated by the local model velocity, is no longer valid. Using linear momentum actuator disc theory however, we derive a relationship between these two velocities and formulate a correction to the enhanced bottom drag formulation that consistently applies a force that remains close to the theoretical value, for all grid sizes down to the turbine scale. In addition, a better understanding of the relation between the model, upstream, and actual turbine velocity, as predicted by actuator disc theory, leads to an improved estimate of the usefully extractable energy. We show how the corrections can be applied (demonstrated here for the models MIKE 21 and Fluidity) by a simple modification of the drag coefficient.

*Corresponding author
Email address: s.kramer@imperial.ac.uk (Stephan C. Kramer)

Keywords: tidal turbines, tidal power, tidal stream, enhanced bottom drag, hydrodynamic modelling, energy resource assessment

1. Introduction

One of the key advantages of tidal energy as a renewable energy source, is the predictable nature of the resource. Methods for the detailed prediction of tidal dynamics using hydrodynamic numerical models have been developed over many years and have been applied for many different purposes. Less well understood is how the placement of tidal energy converters in the flow will modify the existing tidal currents at both local and regional scales [1]. The challenge here is that the detailed flow around a turbine is a three-dimensional phenomenon comprising far smaller length scales than those of the underlying tidal resource. A typical approach therefore is to model the turbine scale flow in a three-dimensional CFD simulation based on a actuator disc, blade element, or actuator-line model (see e.g. Sun et al. [24], Harrison et al. [10], Batten et al. [2], Malki et al. [16], Churchfield et al. [3]). The effects of the turbine in a large scale hydrodynamic model are then parameterised, based on properties extracted from the CFD model.

The main requirements for the turbine parameterisation are the removal of the correct amount of momentum and energy from the flow. As will be argued in this paper (section 6; see also Vogel et al. [26]), if the model applies the correct thrust force, this also ensures that the correct total amount of energy is taken out of the flow. Part of this energy extracted in the model should be interpreted as unresolved mixing losses, so that the energy that can be usefully extracted for power production is not directly available. However, the fact that the correct amount of energy and momentum have been taken out, means that the large scale effect of the turbine on the flow is reasonably well modelled.

It is important to note, that the turbine properties derived in e.g. a CFD model, or from lab experiments, typically consider the placing of a single turbine in uniform background flow. Speed dependent properties are then expressed in

terms of the background velocity, which, because the velocity is slowed down in the presence of a turbine, is available as the undisturbed upstream velocity. In a finite width channel, blockage effects may also affect the resulting thrust curve but can be corrected for (see e.g. Garrett and Cummins [9], Whelan et al. [29]) to derive the thrust curve for an idealised free-standing turbine. In addition, the results may be dependent on the turbulent properties of the flow.

An approach followed in many models, e.g. TELEMAC, MIKE 21, ROMS, FVCOM, is to implement the thrust in the form of an equivalent drag force term. For depth-averaged models this effectively comes down to an increased bottom drag [14, 25, 21, 8, 17] (see however Draper et al. [7], Serhadlıoğlu et al. [23] for an alternative approach, the line momentum sink method, which is based on the application of LMADT entirely at the subgrid level). Three-dimensional models may implement the drag as a force over the entire water column [5], or if the vertical resolution allows it the drag can be applied over a vertical cross section (e.g. Roc et al. [22]), i.e. an idealised actuator disc.

Since the thrust force is given as a function of the upstream velocity, it is important to consider what velocity to use for the equivalent drag force in the model. One option is to probe the numerical velocity solution somewhat upstream of the turbine location. This however brings with it various difficulties such as the question of how far upstream is appropriate, or the fact that the flow upstream might not actually return to the uniform background flow condition that was considered in the CFD model, due to bathymetric changes or the presence of other turbines. Additionally, the use of a non-local velocity is not desirable for numerical and computational purposes: it makes it hard to treat the term implicitly (in the time-integration sense), potentially leading to time step restrictions for stability, and memory access outside of a fixed numerical stencil, or across sub-domains in a domain-decomposed parallel model, is computationally inefficient.

When enough mesh resolution is available, both in the horizontal and vertical dimensions, to resolve the flow through the turbine, the relationship between the upstream velocity and the turbine velocity can be predicted using Linear Mo-

mentum Actuator Disc Theory (LMADT). Using this relationship the quadratic drag law can be reformulated into a function of the local velocity, thus overcoming the difficulties and ambiguities mentioned above. This is the approach followed by Roc et al. [22]. The typical width of a tidal turbine, order 20m, can however be orders of magnitude smaller than the spatial scales of the tidal flow so that resolving an individual turbine may become prohibitively expensive.

If the mesh resolution available is such that computational cells are much larger than the turbine scale, the drag force is necessarily applied over a larger area. In a typical implementation a constant drag is applied over a single cell (the cell that contains the turbine). If the cell size is in fact large enough it may be expected (this will be further investigated in this paper), that the local velocity is not actually affected greatly by the presence of the drag term since the drag force is "smeared" out over a large area and the local cell velocity represents an average of the velocity in a large area around the turbine. In that case the difference between the undisturbed background flow and the local cell velocity may be neglected and the turbine can be implemented as a function of the local velocity.

As will be shown in this paper however, when the mesh resolution is refined closer to the turbine scale, this approximation is no longer tenable as the difference between upstream and local velocity becomes too large. As long as individual turbines are not resolved however, the approach by Roc et al. [22] is also not completely valid because the local velocity is still larger than the theoretical turbine velocity predicted by LMADT. In particular, for depth-averaged models the local velocity will remain higher than the actual turbine velocity even when the horizontal scales are sufficiently resolved because the drag acts on the entire water column and thus the depth-averaged model velocity represents an average of the actual turbine velocity and a higher by-pass velocity above and below the turbine. Even in three-dimensional models the drag force is often applied over the entire water column [5], or limited to one or only a few layers [30, 11], and does not necessarily give an accurate representation of the actual turbine cross-section and thus the model velocity where the drag is

applied is not necessarily equal to the real turbine velocity.

Here we demonstrate how the actuator disc computation may be modified to include the fact that the drag force numerically is applied over a different cross section than the actual turbine. Thus again an analytical relationship can be derived between the undisturbed upstream flow and the local cell velocity, and similarly the drag force can be reformulated as a drag law dependent on the local cell velocity. Like the approach taken by Roc et al. [22], this leads to a correction to the drag law, which in this case depends on the local cell width, and can easily be implemented in existing models, as will be demonstrated here for the Fluidity and MIKE 21 models.

For any numerical modelling study it is important to look at the effect of changing the grid resolution on the results of interest. In the modelling guidelines for tidal resource assessments in [15], a range of grid resolutions is recommended depending on the stage of the resource assessment, ranging from kilometre scale for regional studies, down to a range of 500 m to 50 m for specific site feasibility studies. Since the wake of a turbine is a three-dimensional phenomenon, it is not expected that an accurate description of the near-field flow can be obtained with a depth-averaged model. Nevertheless, such models should be capable of studying far-field effects. This relies on the correct forces and their effect on the large-scale flow being modelled correctly. As this paper shows however, the results of the standard enhanced bottom drag parameterisation of the turbine thrust force will deteriorate as the mesh resolution falls below that of the near-field/wake length scale ($\approx 200 - 300$ m for a typical turbine). The correction proposed in this paper ensures that consistent results can be obtained with grid resolutions smaller than the length scale of the turbine wake, all the way down to the turbine scale.

2. Enhanced bottom drag formulation

In this section we will describe the enhanced bottom drag parameterisation of turbines used in many models [21, 6, 17, 30] and demonstrate some issues

with mesh dependency. We will do this within the framework of MIKE 21 [28], a depth-averaged hydrodynamics model widely used in the marine renewable industry, and an equivalent drag-based implementation in Fluidity, an open source, finite element modelling package [20, 12]. By comparing results between the two models we verify that their implementation is based on the same theory and the same issues are observed.

The aim of the turbine parameterisation is to represent the drag force of the turbine on the flow, which is typically given as:

$$\vec{F}(\vec{u}) = \tfrac{1}{2}\rho C_t(|\vec{u}|)A_t|\vec{u}|\vec{u}, \tag{1}$$

here $\vec{u}$ is the flow velocity, ρ the density of sea water, C_t the dimensionless drag or thrust coefficient, and A_t the effective cross-sectional area of the turbine in the flow. The drag coefficient C_t may itself be a function of speed due to turbine properties such as rating, pitch control and the use of a cut-in speed. As discussed in the introduction the drag law, often derived from a small-scale three-dimensional CFD model, is typically expressed as a function of the undisturbed background flow velocity, which corresponds to the uniform velocity upstream of the turbine in the case of an idealised domain.

The depth-integrated shallow water equations (in conservation form) are given by

$$\frac{\partial H\vec{u}}{\partial t} + \nabla\cdot(H\vec{u}\otimes\vec{u}) + gH\nabla\eta + c_b|\vec{u}|\vec{u} = 0, \tag{2}$$

$$\frac{\partial \eta}{\partial t} + \nabla\cdot(H\vec{u}) = 0, \tag{3}$$

where H is the total water depth between bottom and free surface, elevated at a level $z = \eta$, $\vec{u}$ is the depth-averaged velocity, g the gravitational acceleration and c_b is the bottom friction coefficient, ∇ is the horizontal gradient vector, and t is time.

A local momentum balance in a fixed local horizontal area A is derived by integrating (2) over this area, multiplied by ρ:

$$\frac{d}{dt}\int_A \rho H\vec{u} + \int_{\partial A}\rho H\left(\vec{n}\cdot\vec{u}\right)\vec{u} + \int_A \rho g H\nabla\eta + \int_A c_b\rho|\vec{u}|\vec{u} = 0. \tag{4}$$

The second term represents momentum flux through the boundary ∂A. The third term can be rewritten as an integral of hydrostatic pressure around the three-dimensional water column below A. The last term represents a momentum sink term due to bottom friction.

To implement the turbine thrust force through an enhanced bottom friction, $c_b \rightarrow c_b + c_t$, we need the additional momentum sink to be equal to the force, $\vec{F}(\vec{u})$ in (1). To address the question of which velocity $\vec{u}$ is used to compute $\vec{F}(\vec{u})$, in a first attempt we simply employ the local, depth-averaged velocity and average the force over the area A. Thus, we require that

$$\int_A c_t \rho |\vec{u}| \vec{u} = \frac{\int_A \vec{F}(\vec{u})}{A}. \tag{5}$$

Combined with (1) , it readily follows that the enhanced bottom drag coefficient c_t in this case should be set to:

$$c_t(\vec{u}) = \frac{C_t(\vec{u}) A_t}{2A}. \tag{6}$$

Since we consider the parameterisation of turbines in hydrodynamic models where mesh distances are larger than the size of an individual turbine, the force is applied over the smallest area possible, typically the area of a single mesh cell. Thus the area A in (6) corresponds to the cell area over which the enhanced drag coefficient is applied. In models where the cell area is much larger than the turbine cross section A_t, the additional drag is small and therefore the presence of the turbine will not have a large effect on the numerical solution for $\vec{u}$ in that cell. As an example, for typical values of $C_t = 0.6$, a mesh distance $\Delta x = 200\ m$ and turbine diameter $D = 18\ m$, if the drag is applied over a single square computational cell of $\Delta x \times \Delta x$, we get

$$c_t(\vec{u}) = \frac{C_t \pi \left(\frac{D}{2}\right)^2}{2\Delta x^2} \approx 0.00122, \tag{7}$$

which is only half of a typical value of $c_b = 0.0025$ for the background bottom friction coefficient.

Since the effect of the additional drag is relatively small it is to be expected that the assumption that the local velocity within the cell is close to the undisturbed background flow is valid for relatively coarse resolution models, and can

therefore be used in the averaged force in the right-hand side of (5). As the resolution is increased however and the mesh distances become closer to the turbine scale, the drag is applied over a smaller area and the reduction in local flow speed may become much larger. Because of the quadratic dependency of the drag force on the flow speed, this may have a significant impact on the force that is applied in the model.

3. Local velocity drop in idealised channel

We investigate the mesh-dependent reduction in local flow speed in more detail in the following idealised set up: a turbine is placed in a rectangular channel of length 10 km and width 1 km. The depth at rest is set to 25m and a bottom friction of $c_b = 0.0025$, equivalent to a Chézy coefficient of 62.6 $\mathrm{m}^{1/2}\mathrm{s}^{-1}$, is applied. At the upstream boundary a uniform velocity of 3.0 ms^{-1} is enforced. At the downstream end a Flather boundary condition is applied. The steady state solution without a turbine can be described as a balance between the free surface gradient and the bottom friction. The necessary free surface slope leads to a water level that is approximately 0.9 m higher at the upstream boundary than at the downstream boundary, which in turn (due to the nonlinear continuity equation) leads to an acceleration along the channel with $u \approx 3.12$ ms^{-1} downstream. The velocity at the turbine location, halfway the channel was observed to be approximately 3.055 ms^{-1}.

For the simulations with a turbine, the following turbine parameters were chosen: the thrust coefficient $C_t = 0.6$ with a turbine diameter of $D = 16$ m giving a turbine cross-sectional area of $A_t = 201$ m^2. The simulations were performed using both MIKE 21 and Fluidity on a series of identical triangular meshes with uniform resolutions starting at a mesh size of $\Delta x = 320$ m, doubling the resolution each time with the mesh size decreasing down to $\Delta x = 20$ m, and one final resolution at $\Delta x = D = 16$ m. For the parameterisation of the turbine in Fluidity the enhanced bottom drag approach described in the previous section was used. Although Fluidity here uses a finite element scheme

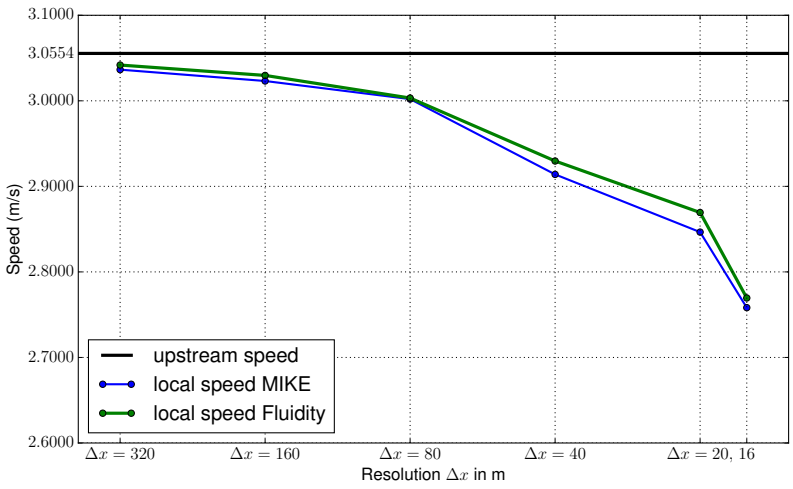

Figure 1: The speed at the turbine location, inside the enhanced bottom drag cell, decreases with increasing resolution both in the Fluidity and MIKE results.

with a discontinuous piecewise linear velocity and piecewise quadratic pressure solution (the mixed $\mathrm{P1_{DG}}-\mathrm{P2}$ formulation, see Cotter et al. [4]) a piecewise constant drag field was used to simplify the computations and to remain close to the numerics of MIKE which uses a finite volume scheme with higher order flux reconstructions. Although the exact details of the implementation in MIKE were not available, the results between Fluidity and MIKE were found to be close enough to extend the analysis based on the parameterisation used in Fluidity to that in MIKE 21.

Figure 1 displays the obtained velocity in the cell in which the drag has been enhanced to parameterise the effect of a turbine. For the cell centred scheme of MIKE 21, cell values were directly available from the model, whereas for Fluidity cell averaged values were computed. It can be seen that the obtained velocity is indeed highly mesh-dependent, and drops with increased mesh resolution. Since the square of this velocity is used to implement the drag term, a 10% drop in the local velocity leads to a 20% drop in the drag force.

In a model of a fully resolved turbine the local velocity is expected to drop

and can be estimated using linear momentum actuator disc theory (LMADT, see [9] for an application of this theory to tidal turbines). The theory assumes inviscid flow and a uniform upstream velocity u_0. Furthermore, it defines a velocity u_1 through the turbine, and velocities u_3 and u_4 in respectively the wake and bypass flow (see figure 3). LMADT also defines pressures: p_0 for the upstream pressure, p_1 and p_2 directly on either side of the turbine, and a uniform pressure p_4 downstream where the velocities u_3 and u_4 are defined. At the same downstream location, the cross-sectional area of the wake flow is defined as A_3. In addition, LMADT defines the known cross sections A_c for the total channel cross section and A_t for the turbine cross section.

Through selective application of the continuity equation, momentum conservation and Bernoulli's principle, seven equations can be derived for the unknowns $u_1, u_3, u_4, p_1, p_2, p_0$ and A_3, given u_0 and p_4 as upstream and downstream boundary conditions respectively (see Appendix A). These equations can be simplified greatly by assuming $A_t \ll A_c$, which means no blockage effects are taken into account. For this case, $u_4 = u_0, p_4 = p_0$ and the velocity through the turbine can be computed as (cf. equation (A.22) in the appendix):

$$u_1 = \tfrac{1}{2}\left(1 + \sqrt{1 - C_t}\right) u_0. \tag{8}$$

For our idealised channel case considered above, we may compute $u_1 = 2.49$ ms^{-1}. As we can see in the figure 1 however, the drop of the velocity in the turbine drag cell is much smaller. This is due to the fact that the force is applied over a larger width than is assumed in the LMADT calculation. In Appendix B it is shown how this calculation can be adjusted to take this into account in addition to the fact that the force applied is based on the local instead of the upstream velocity. In the appendix, the following relation between local cell velocity $\hat{u}_1$ and upstream velocity u_0 is derived:

$$\hat{u}_1 = \frac{1}{1 + \frac{1}{4}\frac{A_t}{\hat{A}_t} C_t} u_0, \tag{9}$$

here $\hat{A}_t = H\Delta y$ is the *numerical* cross-section, which reflects the fact that in a

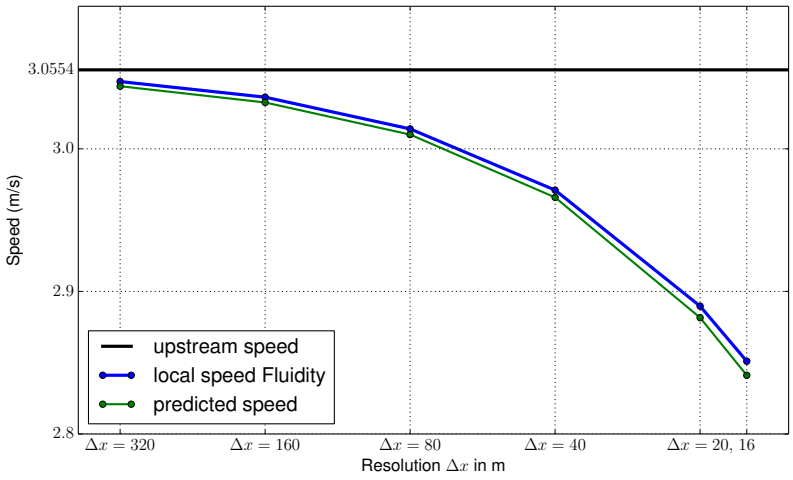

Figure 2: The speed inside a square drag cell decreasing with increasing resolution. Results are model outputs from Fluidity. The plotted speed is the average value over the square area. The decreasing cell speed can be accurately predicted using (9) derived from actuator disc theory.

depth-averaged model the force is effectively applied over the entire water depth H.

Figure 2 shows that the speed predicted by (9) closely follows that computed with Fluidity. It should be noted that in the derivation of (9) we have assumed that the drag is applied over a square area and we are therefore here comparing with Fluidity results on meshes that incorporate a $\Delta x \times \Delta x$ square cell consisting of two triangles, but are unstructured everywhere else. In figure 1 however the Fluidity results were obtained on fully unstructured meshes with the drag applied over the arbitrary triangle that contains the specified turbine location. This is so that it would correspond with the turbine implementation in MIKE. Comparing the two figures it can be seen that the Fluidity results are indeed different. For this reason we first derive a correction for the rectangular drag cell case in the next section, followed by a correction for triangular drag cells in section 5.

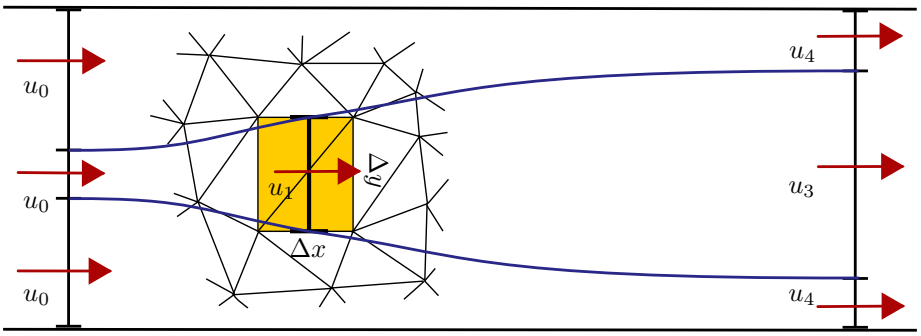

Figure 3: Approximation of the enhanced drag formulation by actuator disc theory. The effect of the enhanced drag is assumed to be equivalent to an actuator disc of width Δy, the width of the cell in the direction transverse to the flow. An upstream velocity u_0 is assumed to reduce to a "turbine" velocity u_1 inside the rectangle, of dimensions $\Delta x \times \Delta y$, in which the enhanced drag is applied. The relation between u_1 and u_0 can be estimated using actuator disc theory which involves eliminating wake and bypass velocities u_3 and u_4 from a set of algebraic equations derived from selectively applying mass and momentum conservation and Bernoulli principles (see Appendix A).

4. Turbine correction for rectangular cells

The aim of the correction is to ensure that we apply the correct force based on a given thrust coefficient C_t:

$$F = \tfrac{1}{2}\rho A_t C_t u_0^2, \tag{10}$$

where u_0 is the upstream velocity which is not readily (and locally) available. We need to take into account that the force in the model is not applied over the cross-section A_t, but is "smeared" horizontally over a rectangle of dimensions $\Delta x \times \Delta y$. Here, the rectangle is assumed to be aligned with the flow with Δx the length of the cell in the streamwise-direction, and Δy the width of the cell in the transverse direction (see figure 3).

In a depth-averaged model the drag force acts over the entire depth H of the water column. This means that it acts acts as an actuator disc with a cross-section of $\hat{A}_t = H\Delta y$ and thickness Δx. If we want to apply LMADT to predict the velocities in our model, we therefore need to apply this cross-section in the

calculation. As usual we neglect the thickness Δx, and assume an infinitely thin disc.

Although the required force is expressed using the actual turbine cross section A_t, the thrust coefficient should be defined using the cross section $\hat{A}_t$ that it is actually applied over in the model:

$$\hat{C}_t := \frac{F}{\frac{1}{2}\rho \hat{A}_t u_0^2} = \frac{A_t}{\hat{A}_t} C_t. \tag{11}$$

Assuming $\hat{u}_1$ is an adequate estimate for the local velocity in the cell with enhanced drag c_t and cell area A, the force applied by the enhanced drag is given by (cf. the left-hand side of (5)):

$$F = \rho A c_t \hat{u}_1^2. \tag{12}$$

Note that here, we cannot use (9) as this was derived based on the assumption that the standard enhanced bottom drag formulation without correction was applied, i.e. the force was different from (10). Using LMADT, taking into account the different cross-sections, and following the same steps in the derivation of (8), we arrive at the same expression but with C_t replaced by $\hat{C}_t$:

$$\hat{u}_1 = \tfrac{1}{2}\left(1 + \sqrt{1 - \hat{C}_t}\right) u_0. \tag{13}$$

After substitution, we write F as a function of the upstream velocity u_0:

$$F = \rho A c_t \tfrac{1}{4}\left(1 + \sqrt{1 - \hat{C}_t}\right)^2 u_0^2. \tag{14}$$

To obtain the appropriate value of c_t we equate this expression with the desired force in (10). This leads to:

$$c_t = \frac{C_t A_t}{2A} \frac{4}{\left(1 + \sqrt{1 - \frac{A_t}{\hat{A}_t} C_t}\right)^2}. \tag{15}$$

In comparison with (6) from the standard enhanced bottom drag formulation, we have obtained an additional factor that corrects for the fact that we are using the local cell velocity instead of the upstream velocity. For coarse resolution runs, we have $A_t/\hat{A}_t \to 0$, and thus we fall back, as expected, to the unmodified enhanced

drag formulation, since the cell velocity is close to the upstream velocity. As we have seen for finer resolutions, still coarser than the turbine scale, the difference between cell and upstream velocities becomes significant.

The correction derived above can also be applied to three-dimensional simulations with a resolved turbine, where the drag force is applied in three-dimensions over a vertical cross-sectional area (actuator disc) with $\hat{A}_t = A_t$ and therefore $\hat{C}_t = C_t$. The correction factor then simplifies to exactly that given by Roc et al. [22]. For the unresolved case however, both in two and three dimensions, the correction derived here not only corrects for the difference between upstream and turbine velocity, but also for the difference between the actual turbine cross-section and the cross-section over which the drag is applied numerically.

Returning to our idealised channel case, in figure 4 it is shown how the force in the standard enhanced bottom drag formulation applied to a square decreases with increasing mesh resolution. It is to be noted that the relative drop in drag force is larger than the relative drop in speed, due to the quadratic dependency of the force on the speed. Adjusting the drag formulation according to (15), the applied force is not only more accurate at coarse resolution, but also remains much closer to that computed from the upstream velocity directly as the mesh resolution approaches the turbine scale.

5. Turbine correction for triangular cells

We now return to the case where the enhanced drag formulation is applied to a single triangular cell, not necessarily aligned in any way with the flow. Again we may approximate the applied drag by an actuator disc spanning the width of the triangle. In this case however, if we thus collapse the applied drag force to a single line, the amount of drag varies along the disc.

We assume here that the streamlines run parallel through the triangle and use a local coordinate system where x is in the streamwise direction and $0 \leq y \leq \Delta y$ in the transversal direction, where Δy is the largest width of the triangle. We

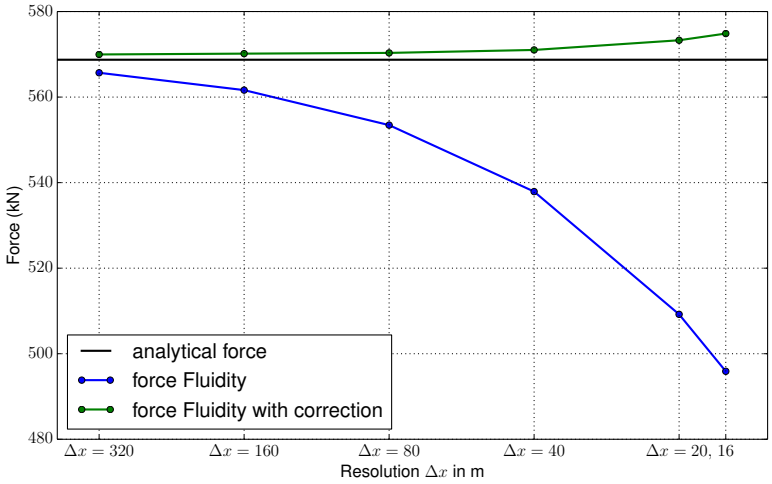

Figure 4: In the standard enhanced drag formulation for tidal turbines, equation (6), the applied force is a quadratic function of the local velocity in the drag cell (here, a square area of $\Delta x \times \Delta x$). As the mesh resolution increases, the local velocity drops, and therefore the force that is applied within the model decreases. Using the correction in (15) however, the same force can be maintained more or less independent of resolution.

may subdivide the triangle into a number of streamtubes of infinitesimal width $\mathrm{d}y$, which can be considered as rectangles $\Delta x \times \mathrm{d}y$, whose length $\Delta x = \Delta x(y)$ is a function of y.

For simplicity we first consider a triangle that is oriented in such a way that it is at its widest at $y = \Delta y$, in other words its top edge is aligned with the streamline at $y = \Delta y$ (see figure 5). Furthermore, we have $\Delta x(y = 0) = 0$ in the bottom vertex, and $\Delta x(y)$ varies linearly for $0 \leq y \leq \Delta y$. Its area can be computed as $A = \frac{1}{2}\Delta x(\Delta y)\Delta y$. The function $\Delta x(y)$ is therefore given by:

$$\Delta x(y) = \frac{2A}{\Delta y^2} y. \tag{16}$$

The force applied in each streamtube is given by

$$\mathrm{d}F = \Delta x(y)\mathrm{d}y\rho c_t \hat{u}_1(y)^2, \tag{17}$$

where $\hat{u}_1(y)$ is the velocity through the streamtube. Similar to (B.2), we apply actuator disc theory where we assume that this force is applied over a cross section $H\mathrm{d}y$ and obtain a modified thrust coefficient:

$$\hat{C}_t := \frac{dF}{\frac{1}{2}\rho H \mathrm{d}y u_0^2} = \frac{2\Delta x(y)dy}{H\mathrm{d}y}\frac{\hat{u}_1^2}{u_0^2} c_t \tag{18}$$

Following the same steps as in equations (B.2)–(9) we may derive the following relation between $\hat{u}_1(y)$ and the upstream velocity u_0:

$$\hat{u}_1(y) = \frac{1}{1 + \frac{1}{2}\frac{\Delta x(y)\mathrm{d}y}{H\mathrm{d}y} c_t} u_0 = \frac{1}{1 + \frac{Ac_t}{H\Delta y^2} y} u_0. \tag{19}$$

The varying width $\Delta x(y)$ thus leads to a variation of the velocity $\hat{u}_1(y)$ for $0 \leq y \leq \Delta y$. In the computer models the accuracy of this variation is limited by the numerical approximations employed.

In MIKE, the underlying discretisation is based on a piecewise-constant velocity in each cell. To estimate the cell average obtained in the model we therefore evaluate (19) at the centroid, $y = \frac{2}{3}\Delta y$, which gives:

$$u_1^{\mathrm{MIKE}} = \frac{1}{1 + \frac{2}{3}\frac{Ac_t}{H\Delta y}} u_0. \tag{20}$$

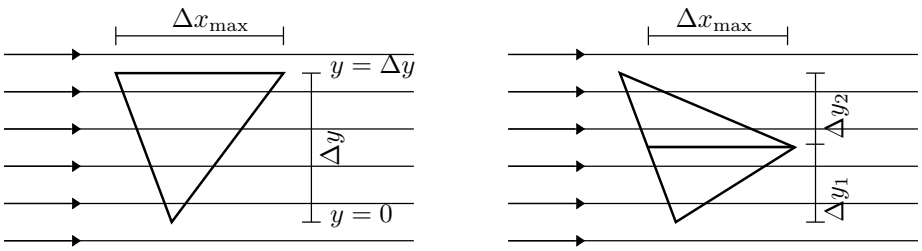

Figure 5: Left figure: a triangle with its top edge aligned with the streamlines. A coordinate reference frame is chosen, with $0 \leq y \leq \Delta y$ the coordinate in the cross-stream direction. The width Δx of the triangle in the streamwise direction, varies as a function of y, starting at $\Delta x(y) = 0$ at $y = 0$, and reaching its maximum width $\Delta x(y) = \Delta x_{\max}$ at $y = \Delta y$. Right figure: a non-aligned triangle can be divided in two triangles that share an edge that *is* aligned with the streamlines. In this case, the maximum width $\Delta x_{\max}$ is the length of the shared edge.

For the case where the triangle does not have one of its edges aligned with a streamline, we may consider splitting the triangle into two triangles that share an edge that *is* aligned along the streamline (see figure 5). The length of this shared edge is the maximum width $\Delta x_{\max}$ of the triangular drag cell in the streamwise direction. The area of either of the two triangles that the cell is split into, can be computed as $A_{1,2} = \frac{1}{2}\Delta x_{\max}\Delta y_{1,2}$, where $\Delta y_{1,2}$ is the height of either triangle. Therefore for each of the triangles we have $A_{1,2}/\Delta y_{1,2} = \frac{1}{2}\Delta x_{\max}$. Thus if we apply the same enhanced friction coefficient c_t in both triangles, it follows that the estimate (20) for the cell average of u_1^{MIKE} is the same in both triangles:

$$u_1^{\text{MIKE}} = \frac{1}{1 + \frac{1}{3}\frac{\Delta x_{\max}}{H}} u_0. \tag{21}$$

Moreover, if we define the overall cross-stream width of the original combined triangle as $\Delta y = \Delta y_1 + \Delta y_2$, we again have $A/\Delta y = \frac{1}{2}\Delta x_{\max}$. Thus, in the actual model where the original, non-aligned triangular drag cell is not split, we can use the same equation (20) for the estimated average velocity of the entire cell as we did for the aligned case.

Using this estimated average, the force applied in the model is then:

$$F = A\rho c_t (u_1^{\mathrm{MIKE}})^2 = A\rho c_t \left(\frac{1}{1 + \frac{2}{3}\frac{Ac_t}{H\Delta y}} \right)^2 u_0^2. \tag{22}$$

By equating this to the desired force (1), we may derive a quadratic expression for c_t

$$-2A^2 A_t C_t c_t^2 + A\left(9H^2\Delta y^2 - 6A_t C_t H \Delta y\right) c_t - \tfrac{9}{2} A_t C_t H^2 \Delta y^2 = 0 \tag{23}$$

In Fluidity, the $\mathrm{P1_{DG}}$-discretisation prescribes a linear variation for velocity. Thus we approximate (19) by evaluating it at $y = 0$ and $y = \Delta y$ and assuming a linear variation in between:

$$u_1^{\mathrm{Fluidity}}(y) = \left(1 - \frac{1}{1 + \frac{H\Delta y}{Ac_t}} \frac{y}{\Delta y} \right) u_0 \tag{24}$$

The force applied in the model can be found by integrating:

$$F = \int_{y=0}^{\Delta y} \Delta x(y) \rho c_t (u_1^{\mathrm{Fluidity}}(y))^2 \mathrm{d}y \tag{25}$$

$$= A\rho c_t \left(1 - \tfrac{4}{3} \left(\frac{1}{1 + \frac{H\Delta y}{Ac_t}} \right) + \tfrac{1}{2} \left(\frac{1}{1 + \frac{H\Delta y}{Ac_t}} \right)^2 \right) u_0^2. \tag{26}$$

Equating with the desired force in (1) this time results in a cubic expression for c_t:

$$A^3 c_t^3 + A^2 \left(4H\Delta y - 3A_t C_t\right) c_t^2 + 6A\left(H^2\Delta y^2 - A_t C_t H \Delta y\right) c_t - 3A_t C_t H^2 \Delta y^2 = 0. \tag{27}$$

In case the triangular drag cell does not have an edge that is aligned with the streamlines, we may again consider splitting it into two triangles with a shared edge that is aligned with the flow. Here however, (24) does not predict the same linear function for u_1^{Fluidity} in both triangles, since although $A/\Delta y = \frac{1}{2}\Delta x_{\max}$ is the same, the value for Δy in the denominator of $y/\Delta y$ is different for both triangles, and due to the different orientation of the top triangle, the sign of the gradient of u_1^{Fluidity} with respect to y will be opposite. The combined piecewise

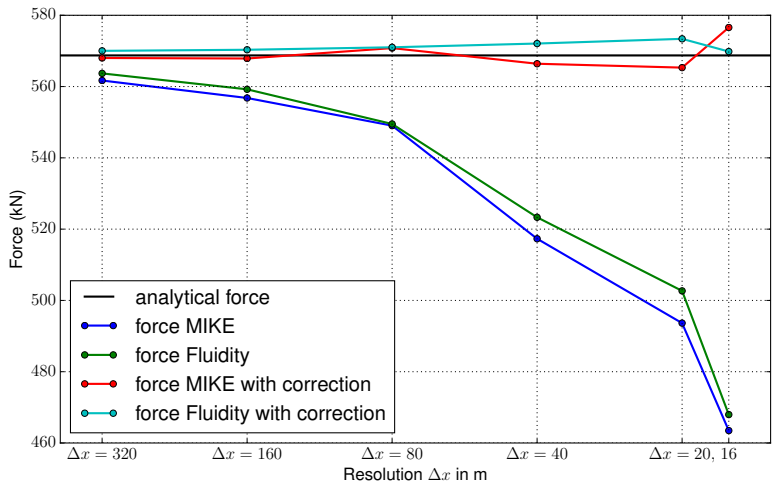

Figure 6: Results for the enhanced drag formulation with the drag applied in a single triangular cell as implemented in both Fluidity and MIKE 21. As in figure 4, which show the results for the rectangular case, the force applied decreases significantly with increasing mesh resolution. Applying the correction for c_t however, given by solving (23) (MIKE 21) or (27) (Fluidity), the force can be kept more or less constant and much closer to the desired value.

solution is therefore not supported by the underlying discretisation. However, we did find that when using the value of c_t found by solving (27), the discrete model gave results that varied only slightly for different orientations of the triangular cell.

The results in figure 6 indicate that again the force applied in the unmodified enhanced drag implementation, in Fluidity and MIKE reduces significantly with increasing mesh resolution. A modification to the enhanced bottom drag c_t was derived in this section, solving for c_t in (23) and (27) for MIKE and Fluidity respectively, that is shown here to lead to a force that remains close to the desired value. The correction in MIKE was implemented by first finding the value for c_t from (23) and then working back from (6) to compute what value of C_t should be entered in the GUI to achieve this value in MIKE.

6. Power production

The correction to the enhanced drag formulation, derived in this paper, is to ensure that the correct amount of momentum is extracted from a shallow water model. This means that the force F applied by the enhanced drag in the drag cell (or region) is an accurate approximation of the real thrust exerted by the turbine on the flow. The amount of energy taken out of the flow within the cell is given by:

$$P_{\text{cell}} = F\hat{u}_{1,\text{model}}, \tag{28}$$

where $\hat{u}_{1,\text{model}}$ is the velocity in the enhanced drag cell. As we have seen however, in the case where turbines are not fully resolved this velocity will be larger than the actual velocity $u_{1,\text{turbine}}$ that goes through the turbine (as predicted by actuator disc theory). Therefore, the real power production $P_{\text{turbine}} = Fu_{1,\text{turbine}}$ will be smaller than the amount of power P_{cell} taken out of the model in the drag cell.

This discrepancy can be explained from the fact that part of the mixing losses are not modelled explicitly within the model, but occurs at the sub-grid scale. Following the analysis of Vogel et al. [26], the total amount of power taken out of the flow can be split as follows:

$$P_{\text{total}} = P_{\text{turbine}} + P_{\text{mixing}}, \tag{29}$$

where P_{mixing} takes account of the mixing losses due to a.o. shear between the wake and bypass flows. The total power can be computed as [26]:

$$P_{\text{total}} = Fu_0. \tag{30}$$

Therefore, as long as the model applies an accurate representation of the thrust force F, using the correction presented in this paper, and an accurate value for the upstream velocity u_0, the total power extracted from the flow in the model will be accurate as well. The fact that the power P_{cell} extracted within the drag cell, according to (28), is larger than P_{turbine} means that the mixing loss that occurs in the model (outside the drag cell) must be smaller than the

real P_{mixing} predicted by actuator disc theory. Therefore part of the mixing loss occurs within the drag cell itself. Thus P_{cell} accounts for both the power P_{turbine} taken out by the turbine itself and additional losses that happen at the sub-grid level.

Vogel et al. [26] considers the case where the drag of an entire farm is smeared out over an enhanced drag region, with the assumption that all mixing losses actually occur within this region. In that case it may be assumed that the total power extraction in the model is a good approximation of the total power extraction predicted by actuator disc theory, so that the available usefully extracted power can be computed as a fraction of that using the same theory.

For the case, considered in this paper, where individual turbines are modelled but are not necessarily fully resolved, part of the mixing losses are modelled explicitly. As argued above however, using the power extracted from the flow by the turbine parameterisation still leads to an overprediction of the usefully extractable energy. It is to be noted that in a shallow water model, even if an individual turbine is resolved in the horizontal mesh, with a minimum mesh distance smaller or equal than the turbine diameter D, the effective cross-section $\hat{A}_t = \Delta y H$ will still be larger than the actual turbine cross-section A_t. This is because the actual cross-section does not span the entire depth of the water. Thus, the velocity at the turbine in the model should be interpreted as a depth-averaged velocity that averages between the velocity through the turbine, and the bypass velocity above and below the turbine. This velocity is therefore expected to be higher than the real turbine velocity itself, and therefore the power extraction by the depth-averaged turbine-parameterisation will always be an overprediction of the actual power available to the turbine. The difference between these power values roughly corresponds to vertical mixing losses that are not explicitly modelled in the depth-averaged model. In the next section we will explain how the relationship between the upstream velocity and the local velocity in the model, derived in this paper, can also be used to predict the usefully extractable energy, excluding mixing losses, more accurately.

7. Conclusions

In order to estimate accurately the resource available to tidal turbines and to assess their impact on the hydrodynamics, it is important to represent properly the drag force exerted by the turbines on the flow. In depth-averaged, and more generally under-resolved hydrodynamic models, one should keep in mind that the local model velocity at the turbine is different from both the upstream and the actual velocity passing through the turbine. The relationship between them is dependent on the mesh resolution, and in the case of depth-averaging, the ratio between the actual turbine cross section and the flow cross section spanning the entire depth. Therefore, although the use of the local velocity for the implementation of the drag force is computationally attractive, it is required to take these relationships into account to avoid spurious and mesh-dependent results. In addition, a better understanding of the relation between local and upstream velocity is necessary for an accurate estimate of the power available to the turbine.

Here we have presented the theory for a single, isolated turbine, and demonstrated that a correction based on linear momentum actuator disc theory taking into account the actual numerical cross section that the force is applied over in the model, can be used to obtain results that are consistent over a range of grid scales. It was shown that the standard enhanced bottom drag formulation results in a drag force that decreases with decreasing grid lengths, in particular when the grid size falls below the length scale of the turbine wake (roughly 10–20 turbine diameters). With the correction the applied force can be kept constant to a large degree, thus ensuring that the effect of the turbine on the large scale flow is correctly modelled.

The analysis for single, isolated turbines may be sufficient for sparsely populated turbine sites which see little interaction between turbines. It is generally recognised however, that in order to achieve the maximum available energy from certain sites, one needs to consider turbine configurations that benefit from local and global blockage effects [18], e.g. fence structures. It should be pointed

out that depending on resolution, the hydrodynamic model already takes into account blockage effects. In three dimensions, if the turbines are fully resolved, an accurate estimate of the local turbine velocity is available. Therefore if we assume that the force can be expressed as a function of local properties, blockage effects should also be dealt with correctly. This is the approach taken by Roc et al. [22], and as we have shown here, the correction to the enhanced drag approach converges to this formulation in the limit of a fully resolved turbine in three dimensions.

For the under-resolved case, the difference between the actual turbine cross-section and the numerical cross-section in the model may also influence the accuracy of, in particular, local blockage effects. The correction could potentially be improved by taking this difference into account. If the turbine force is expressed as a function of the actual local turbine velocity, and assuming this expression remains valid for different blockage ratios, this can be achieved in two steps. First, we use LMADT, without taking the low blockage limit, to reformulate it as a blockage-dependent function of the upstream velocity (see e.g. Garrett and Cummins [9], Whelan et al. [29]). Then this expression can again be reformulated, now as a function of the local velocity in the drag cell using LMADT that takes into account blockage based on the numerical cross-section. The significance of such a further correction is yet to be determined in numerical tests, and is part of planned future work. As argued above however the correction in this paper will lead to the correct blockage behaviour in the limit of a resolved turbine, in other words it converges to the correct answer. The uncorrected standard enhanced drag approach on the other hand will converge to an answer that is incorrect in both low and high blockage cases.

Finally, for local blockage effects that take place entirely at the subgrid level, e.g. multi-rotor devices and (partial) fences of turbines, further analysis is needed to derive a relation between thrust and upstream velocity that takes local blockage into account. This could be achieved using a number of approaches including lab experiments and more detailed CFD simulations with combined devices, as well as with analytical approaches such as in [18] and [19]. There it

was shown how in a partial fence of turbines, the relation between thrust and velocity upstream of a single turbine, can be combined into a relation between the total thrust of the fence and a velocity upstream of the fence. This thrust curve for the fence can then be used to treat it as a single device when implementing it in a hydrodynamic model. It should however be emphasised that knowledge of the local-blockage dependent thrust curve is not sufficient for a correct implementation. As for the single device case, it should be combined with the predicted relation, derived in this paper, between upstream and local cell velocity which is dependent on the numerical properties of the model, in particular mesh resolution.

With more closely packed turbines the representation of turbine wake structures and wake recovery also becomes much more important. In addition, the turbulence characteristics may have a great impact on the performance of the turbines. As mentioned in the introduction, depth-averaged models will not be sufficient to accurately model these three-dimensional near-field effects. In further work we would like to explore however, how well these effects can still be approximated in depth-averaged models, possibly through parameterisation and tuning of horizontal turbulence models. Nonetheless, we recognise that in general it may no longer be possible to simply extrapolate from the results of a single isolated turbine, and it may be required to study the effects of combining multiple turbines in detailed three-dimensional CFD calculations and lab experiments.

8. Acknowledgements

The authors would like to kindly acknowledge the UK's Engineering and Physical Sciences Research Council (EPSRC), projects EP/J010065/1 and EP/M011054/1, for funding which supported this work. Part of the computations in this work have been made possible using the Imperial College High Performance Computing Service.

Appendix A. Linear Momentum Actuator Disc Theory

In this appendix we briefly review the main steps in the derivation of the actuator disc theory used in tidal turbine calculations. This is so we can refer to the relevant equations when the modifications, that take into account the numerical implementation details of the enhanced bottom drag formulation, are derived in the main text. These results can be found in e.g. Garrett and Cummins [9], or Whelan et al. [29].

We consider a channel of cross-sectional area A_c in which a turbine is located with cross section A_t. We assume a uniform flow across the channel upstream of the turbine with velocity u_0, the flow through the turbine is u_1. Further downstream we define u_3 to be the velocity in the wake, and u_4 the bypass velocity. Furthermore we assume that at the point down-stream where u_3 and u_4 are defined we have a uniform water level η_4. The water level upstream is denoted by η_0, and the water levels just upstream and downstream of the turbine, associated with the pressure drop across the turbine are denoted by η_1 and η_2.

First we formulate the conservation of mass for the flow through the turbine and in the bypass flow

$$A_t u_1 = A_3 u_3, \tag{A.1}$$

$$A_c u_0 = A_3 u_3 + (A_c - A_3) u_4, \tag{A.2}$$

where A_3 is the cross-sectional area of the wake at the location where u_3 is defined. Here we neglect the influence of the water level on the cross sections, so that the cross-sectional area of the bypass flow is given by $A_c - A_3$. Inclusion of the dependency of cross section on the water level is only significant for high Froude numbers, with details given in [29].

The force F exerted by the turbine on the flow (and vice-versa), can be related to a conservation of momentum principle in the entire channel, or to the

pressure drop across the turbine:

$$F = A_c \rho u_0^2 - A_3 \rho u_3^2 - (A_c - A_3)\rho u_4^2 + \rho g A_c(\eta_0 - \eta_4), \tag{A.3}$$

$$F = \rho g A_t(\eta_1 - \eta_2), \tag{A.4}$$

where g is the gravitational acceleration. Finally, applying Bernoulli's principle along streamlines: 1) from upstream, where u_0 is considered uniform, to just before the turbine, where water level η_1 is defined; 2) from just after the turbine, where water level η_2 is defined, to downstream where a uniform water level η_4 is defined; and 3) in the bypass flow from upstream to downstream. This yields three more equations:

$$\tfrac{1}{2}u_0^2 + g\eta_0 = \tfrac{1}{2}u_1^2 + g\eta_1, \tag{A.5}$$

$$\tfrac{1}{2}u_1^2 + g\eta_2 = \tfrac{1}{2}u_3^2 + g\eta_4, \tag{A.6}$$

$$\tfrac{1}{2}u_0^2 + g\eta_0 = \tfrac{1}{2}u_4^2 + g\eta_4. \tag{A.7}$$

Assuming boundary conditions for u_0 and η_4, and an expression for F as a function of u_0, we have seven equations for seven unknowns: $u_1, u_3, u_4, \eta_0, \eta_1, \eta_2$, and A_3.

General solutions

The Bernoulli equations (A.5) to (A.7) can be rewritten as expressions for water level differences:

$$g\eta_1 - g\eta_2 = g\eta_0 - g\eta_4 + \tfrac{1}{2}\left(u_0^2 - u_3^2\right), \tag{A.8}$$

$$g\eta_0 - g\eta_4 = \tfrac{1}{2}\left(u_4^2 - u_0^2\right), \tag{A.9}$$

and thus

$$g\eta_1 - g\eta_2 = \tfrac{1}{2}\left(u_4^2 - u_3^2\right). \tag{A.10}$$

We can therefore rewrite the two expressions (A.3) and (A.4) as:

$$F = A_3\rho\left(u_4^2 - u_3^2\right) - \tfrac{1}{2}A_c\rho\left(u_4^2 - u_0^2\right) \tag{A.11}$$

$$F = \tfrac{1}{2}A_t\rho\left(u_4^2 - u_3^2\right) \tag{A.12}$$

Equations (A.2), (A.11) and (A.12) give three equations for the three unknowns u_3, u_4 and A_3. Substitution of $A_3(u_4 - u_3) = A_c(u_4 - u_0)$ from (A.2), in (A.11) eliminates A_3:

$$\begin{aligned} F &= A_3\rho\left(u_4 - u_3\right)\left(u_4 + u_3\right) - \tfrac{1}{2}A_c\rho\left(u_4^2 - u_0^2\right) \\ &= A_c\rho\left(u_4 - u_0\right)\left(u_4 + u_3\right) - \tfrac{1}{2}A_c\rho\left(u_4^2 - u_0^2\right) \\ &= A_c\rho\left(u_4 - u_0\right)\left(u_3 + \tfrac{1}{2}u_4 - \tfrac{1}{2}u_0\right). \end{aligned} \tag{A.13}$$

We can rearrange (A.12) and (A.13) in the following manner, respectively:

$$A_c^2\left(u_4 - u_0\right)^2 u_3^2 = A_c^2\left(u_4 - u_0\right)^2\left(u_4^2 - \frac{2F}{A_t\rho}\right), \tag{A.14}$$

$$A_c^2\left(u_4 - u0\right)^2 u_3^2 = \rho^{-2}\left(F - \tfrac{1}{2}A_c\rho\left(u_4 - u_0\right)^2\right)^2. \tag{A.15}$$

We introduce the additional definitions,

$$C_t := \frac{F}{\frac{1}{2}A_t\rho u_0^2}, \quad \text{and} \quad \epsilon := \frac{A_t}{A_c}. \tag{A.16}$$

Note that we do not have to assume that F is actually quadratic in u_0, so that C_t is not necessarily a constant; it may still be dependent on u_0. With these we can derive the following quartic polynomial in u_4 from (A.14) and (A.15):

$$\frac{1}{4}\left(C_t\epsilon - \left(\frac{u_4}{u_0} - 1\right)^2\right)^2 - \left(\frac{u_4}{u_0} - 1\right)^2\left(\frac{u_4^2}{u_0^2} - C_t\right) = 0. \tag{A.17}$$

Finally, by (A.12):

$$u_3 = \sqrt{u_4^2 - C_t u_0^2}, \tag{A.18}$$

and A_3 can be derived by again substituting (A.2) in (A.11) but this time to eliminate $A_c(u_4 - u0)$, so that

$$F = A_3\rho\left(u_4 - u_3\right)\left(u_3 + \tfrac{1}{2}u_4 - \tfrac{1}{2}u_0\right), \tag{A.19}$$

which in combination with (A.12), gives:

$$A_3 = \frac{\frac{1}{2}u_4 + \frac{1}{2}u_3}{u_3 + \frac{1}{2}u_4 - \frac{1}{2}u_0}A_t. \tag{A.20}$$

Zero blockage limit

From the above, it follows that in the limit $\epsilon \to 0$: $u_4 \to u_0$ and thus $\eta_4 \to \eta_0$. In this limit, (A.18) becomes

$$u_3 \to \sqrt{1 - C_t}\; u_0, \tag{A.21}$$

and combining (A.20) and (A.1):

$$u_1 = \frac{\frac{1}{2}u_4 + \frac{1}{2}u_3}{u_3 + \frac{1}{2}u_4 - \frac{1}{2}u_0} u_3 \to \tfrac{1}{2}\left(1 + \sqrt{1 - C_t}\right) u_0. \tag{A.22}$$

The energy yield then becomes:

$$P = F u_1 \to \tfrac{1}{4}\left(1 + \sqrt{1 - C_t}\right) C_t A_t \rho u_0^3. \tag{A.23}$$

The maximum yield as a function of C_t is obtained by:

$$\frac{d}{dC_t}\left[\left(1 + \sqrt{1 - C_t}\right) C_t\right] = \frac{1 - \frac{3}{2}C_t + \sqrt{1 - C_t}}{\sqrt{1 - C_t}} = 0 \tag{A.24}$$

$$\implies \left(\tfrac{3}{2}C_t - 1\right)^2 = 1 - C_t \implies C_t = \frac{8}{9} \tag{A.25}$$

Thus the maximum power (assuming no blockage) is

$$P_{\max} = \frac{16}{27} \cdot \tfrac{1}{2} A_t \rho u_0^3 \approx 0.59 \cdot \tfrac{1}{2} A_t \rho u_0^3. \quad \textbf{(Betz limit)} \tag{A.26}$$

Appendix B. Predicting the reduced velocity in the enhanced drag cell

Here we show that LMADT can be used to predict the local cell velocity in the standard enhanced drag formulation. When we neglect variations in the streamwise-direction (here denoted as the x-direction), the results of the drag force applied in a shallow water model can be approximated by an infinitely thin actuator disc with a cross-sectional area of $\Delta y H$. Here, and in the rest of the paper, Δy is the width of the drag area, in the cross-stream direction.

Following the assumption made above (5), the magnitude of the force applied in the enhanced bottom drag approximation is given by:

$$F = \tfrac{1}{2}\rho A_t C_t \hat{u}_1^2. \tag{B.1}$$

Note that here we need to use the actual turbine cross section A_t as that is the user input in this formulation to calculate the enhanced drag c_t in (6). Further we assume that the velocity used to compute the force in this approximation, which is simply the local velocity in the drag cell, will be accurately predicted as the velocity $\hat{u}_1$ in the modified actuator disc theory that follows below.

Following the steps in the derivation of (8), (A.22) in the appendix, but now applied to an actuator disc of cross section $\hat{A}_t = \Delta y H$, we first define a modified thrust coefficient (cf. (A.16) in the appendix):

$$\hat{C}_t := \frac{F}{\frac{1}{2}\rho \hat{A}_t u_0^2} = \frac{A_t}{\hat{A}_t}\frac{\hat{u}_1^2}{u_0^2} C_t. \tag{B.2}$$

Following the same derivation of (8), we then obtain a relation between the local model velocity $\hat{u}_1$ and the upstream velocity u_0 if in (8) we replace C_t with $\hat{C}_t$. This gives an expression for the ratio $\hat{u}_1/u_0$ that can be substituted in (B.2), to give:

$$\hat{C}_t = \frac{A_t}{\hat{A}_t}\left(\frac{1}{2}\left(1+\sqrt{1-\hat{C}_t}\right)\right)^2 C_t. \tag{B.3}$$

After some algebraic manipulation[1], this can be reworked to

$$\hat{C}_t = \frac{\frac{A_t}{\hat{A}_t} C_t}{\left(1+\frac{1}{4}\frac{A_t}{\hat{A}_t} C_t\right)^2}. \tag{B.4}$$

Finally, the relation between the local velocity $\hat{u}_1$ within the cell that the enhanced drag is applied in, and the upstream velocity u_0 is given by

$$\hat{u}_1 = \frac{1}{1+\frac{1}{4}\frac{A_t}{\hat{A}_t} C_t} u_0. \tag{B.5}$$

Appendix C. Implementation details

In this appendix we summarise, how the analysis derived in this paper can be practically applied in existing models.

[1] the authors made use of SymPy, a python library for symbolic mathematics: `www.sympy.org`

Turbine drag applied over a rectangular area

For models where the turbine parameterisation consists of an enhanced bottom drag applied over a fixed, rectangular area A (e.g. [25]), we may use the analysis presented in section 4. Where existing models typically make no distinction between upstream and local turbine velocity, they calculate the enhanced drag coefficient as $c_t = C_t A_t / 2A$. Such implementations can be improved using the correction given by (15). The extra factor at the end of (15) can easily be included by the user in either C_t or A_t, without the need for code modification, if these are the input parameters to the model.

An additional complexity arises if C_t itself is not a constant. This occurs for example if a cut-in speed and/or rating are applied to the turbine. In this case, C_t is typically given as a function (thrust curve) of the upstream velocity u_0. In the model however only the local velocity $\hat{u}_1$ is available. Using the formula

$$\hat{u}_1 = \tfrac{1}{2}\left(1 + \sqrt{1 - \hat{C}_t}\right) u_0, \quad \hat{C}_t = \frac{A_t}{\hat{A}_t} C_t, \tag{C.1}$$

however, it is straight-forward to transform a lookup table that gives the thrust coefficient for different values of u_0, into a lookup table that is a function of $\hat{u}_1$, by computing $\hat{u}_1$ for the given values of u_0 as a pre-processing step.

For the computation of the power available to the turbine, we may use (A.23). Here, again we use (C.1) to derive the upstream velocity u_0 from the local cell velocity $\hat{u}_1$. Combining these two equations, we derive:

$$P_{\text{turbine}} = \frac{2\left(1 + \sqrt{1 - C_t}\right)}{\left(1 + \sqrt{1 - \hat{C}_t}\right)^3} C_t \rho A_t \hat{u}_1^3. \tag{C.2}$$

Again, in the case that C_t is not a constant, a lookup table may be used to obtain the correct value of P_{turbine} for each value of $\hat{u}_1$.

Turbine parameterisation in an arbitrary triangular mesh

For models such as MIKE 21 and Fluidity that employ triangular meshes and which implement turbines through an increased drag applied within a single triangle, the theory presented in section 5 can be applied. In triangular mesh

models where the drag force is based on a cell-averaged velocity, the value for the enhanced drag coefficient can be found by solving (23) for c_t. Models that use a linear interpolation of velocities stored in the vertices, such as Fluidity should use the value of c_t found by solving (27). The same approach could also be followed to implement a turbine in a single drag cell in Telemac 2D, where its Finite Element modus is expected to behave in a similar manner as Fluidity, using a linear representation of the velocity within a cell.

In models, like MIKE, where the applied drag force and the associated coefficient c_t are not explicitly prescribed, the same effect can be achieved by modifying the value of C_t. This is done by assuming the implementation is equivalent to the standard enhanced bottom drag formulation according to equation (6). Indeed the results in figure 1 where the standard drag implementation of Fluidity is compared with results in MIKE show that this is true to at least a good approximation. By providing MIKE with a modified value of C_t

$$C_{t,\text{modified}} = \frac{2Ac_t}{A_t}, \tag{C.3}$$

we can therefore create the effect of applying a value of c_t obtained from (23) without modifying the code. Note, that in equation (23) we use the original value of C_t for the real turbine.

For non-constant C_t that is given as a thrust curve, MIKE (and similar models) use the local cell velocity $\hat{u}_1$ instead of the upstream velocity to look up the value of C_t. This can be corrected by converting the upstream values u_0 in a $u_0 \rightarrow C_t$ look-up table into cell velocities $\hat{u}_1$ using equation (20).

To compute the power that can be usefully extracted by the turbine we again use (A.23) this time combined with (20), giving:

$$P_{\text{turbine}} = \tfrac{1}{4}\left(1+\sqrt{1-C_t}\right) C_t A_t \left(1+\tfrac{2}{3}\frac{Ac_t}{H\Delta y}\right)^3 (u_1^{\text{MIKE}})^3. \tag{C.4}$$

For finite element models, such as Fluidity, that consider a linear variation of the velocity within the cell we can use (24) which predicts the relationship between the upstream velocity and the velocity in the cell as a function of y. By first taking an average of the finite element solution u_1^{Fluidity} within the drag

cell in the streamwise direction (x-direction), we can then use this equation to estimate the upstream velocity u_0. This estimate may in practice still vary in the cross-streamwise direction (y-direction), so we take the cell average of its cube to obtain an estimate for u_0^3 in (A.23). Combining all this gives:

$$P_{\text{turbine}} = \tfrac{1}{4}\left(1+\sqrt{1-C_t}\right)\rho\frac{C_t A_t}{A}\int_{y=0}^{\Delta y}\Delta x(y)\left(\frac{\frac{\int_{x=0}^{\Delta x(y)} u_1^{\text{Fluidity}} dx}{\Delta x(y)}}{1-\frac{1+H\Delta y}{Ac_t}\frac{y}{\Delta y}}\right)^3 dy. \quad \text{(C.5)}$$

A practical implementation in Matlab of the correction in three dimensions for users of MIKE 3 is described by Waldman et al. [27]. This is based on the square correction derived in this paper, which was also briefly described in Kramer et al. [13]. The implementation automatically adjusts the input parameters to MIKE 3 and updates them to take into account a variation in flow directions, and the possible movement of vertical layers.

[1] Adcock, T. A. A., Draper, S., Nishino, T., 2015. Tidal power generation – a review of hydrodynamic modelling. Proceedings of the Institution of Mechanical Engineers, Part A: Journal of Power and Energy, 0957650915570349.

[2] Batten, W. M. J., Harrison, M. E., Bahaj, A. S., 2013. Accuracy of the actuator disc–RANS approach for predicting the performance and wake of tidal turbines. Philosophical Transactions of the Royal Society A: Mathematical, Physical and Engineering Sciences 371 (1985), 20120293.

[3] Churchfield, M. J., Li, Y., Moriarty, P. J., 2013. A large-eddy simulation study of wake propagation and power production in an array of tidal-current turbines. Philosophical Transactions of the Royal Society A: Mathematical, Physical and Engineering Sciences 371 (1985), 20120421.

[4] Cotter, C. J., Ham, D. A., Pain, C. C., 2009. A mixed discontinuous/continuous finite element pair for shallow-water ocean modelling. Ocean Modelling 26 (1-2), 86–90.

[5] Defne, Z., Haas, K. A., Fritz, H. M., 2011. Numerical modeling of tidal currents and the effects of power extraction on estuarine hydrodynamics along the Georgia coast, USA. Renewable Energy 36 (12), 3461–3471.

[6] Divett, T., Vennell, R., Stevens, C., 2013. Optimization of multiple turbine arrays in a channel with tidally reversing flow by numerical modelling with adaptive mesh. Philosophical Transactions of the Royal Society A: Mathematical, Physical and Engineering Sciences 371 (1985), 20120251.

[7] Draper, S., Houlsby, G. T., Oldfield, M. L. G., Borthwick, A. G. L., 2010. Modelling tidal energy extraction in a depth-averaged coastal domain. IET renewable power generation 4 (6), 545–554.

[8] Funke, S. W., Farrell, P. E., Piggott, M. D., 2014. Tidal turbine array optimisation using the adjoint approach. Renewable Energy 63, 658–673.

[9] Garrett, C., Cummins, P., 2007. The efficiency of a turbine in a tidal channel. Journal of Fluid Mechanics 588, 243–251.

[10] Harrison, M. E., Batten, W. M. J., Myers, L. E., Bahaj, A. S., 2010. Comparison between CFD simulations and experiments for predicting the far wake of horizontal axis tidal turbines. IET Renewable Power Generation 4 (6), 613–627.

[11] Hasegawa, D., Sheng, J., Greenberg, D. A., Thompson, K. R., 2011. Far-field effects of tidal energy extraction in the Minas Passage on tidal circulation in the Bay of Fundy and Gulf of Maine using a nested-grid coastal circulation model. Ocean Dynamics 61 (11), 1845–1868.

[12] Imperial College London, Applied Modelling and Computation Group (AMCG), 2015. Fluidity manual v4.1.12.
URL `http://dx.doi.org/10.6084/m9.figshare.1387713`

[13] Kramer, S. C., Piggott, M. D., Hill, J., Kregting, L., Pritchard, D., Elsaesser, B., 2014. The modelling of tidal turbine farms using multi-scale, un-

structured mesh models. In: Proceedings of the 2nd International Conference on Environmental Interactions of Marine Renewable Energy Technologies, (EIMR2014), Stornoway, Scotland, www.eimr.org, EIMR2014-7118.

[14] Lalander, E., Leijon, M., 2009. Numerical modeling of a river site for in–stream energy converters. In: Proceedings of the 8th European Wave and Tidal Energy Conference (EWTEC). p. 826832.

[15] Legrand, C., 2009. Assessment of tidal energy resource: Marine renewable energy guides. Tech. rep., European Marine Energy Centre (EMEC).

[16] Malki, R., Williams, A. J., Croft, T. N., Togneri, M., Masters, I., 2013. A coupled blade element momentum–computational fluid dynamics model for evaluating tidal stream turbine performance. Applied Mathematical Modelling 37 (5), 3006–3020.

[17] Martin-Short, R., Hill, J., Kramer, S. C., Avdis, A., Allison, P. A., Piggott, M. D., 2015. Tidal resource extraction in the Pentland Firth, UK: Potential impacts on flow regime and sediment transport in the Inner Sound of Stroma. Renewable Energy 76, 596–607.

[18] Nishino, T., Willden, R. H. J., 2012. The efficiency of an array of tidal turbines partially blocking a wide channel. Journal of Fluid Mechanics 708, 596.

[19] Nishino, T., Willden, R. H. J., 2013. Two-scale dynamics of flow past a partial cross-stream array of tidal turbines. Journal of Fluid Mechanics 730, 220–244.

[20] Piggott, M. D., Gorman, G. J., Pain, C. C., Allison, P. A., Candy, A. S., Martin, B. T., Wells, M. R., 2008. A new computational framework for multi-scale ocean modelling based on adapting unstructured meshes. International Journal for Numerical Methods in Fluids 56 (8), 1003–1015.

[21] Plew, D. R., Stevens, C. L., 2013. Numerical modelling of the effect of turbines on currents in a tidal channel – Tory Channel, New Zealand. Renewable Energy 57, 269–282.

[22] Roc, T., Conley, D. C., Greaves, D., 2013. Methodology for tidal turbine representation in ocean circulation model. Renewable Energy 51, 448–464.

[23] Serhadlıoğlu, S., Houlsby, G. T., Adcock, T. A. A., Draper, S., Borthwick, A. G. L., 2013. Assessment of tidal stream energy resources in the UK using a discontinuous Galerkin finite element scheme. In: 17th Int. Conf. on Finite Elements in Flow Problems, San Diego, CA, 24–27 February 2013.

[24] Sun, X., Chick, J. P., Bryden, I. G., 2008. Laboratory-scale simulation of energy extraction from tidal currents. Renewable Energy 33 (6), 1267–1274.

[25] Vennell, R., 2010. Tuning turbines in a tidal channel. Journal of Fluid Mechanics 663, 253–267.

[26] Vogel, C. R., Willden, R. H. J., Houlsby, G. T., 2013. A correction for depth-averaged simulations of tidal turbine arrays. In: Proceedings of the 10th European Wave and Tidal Energy Conference (EWTEC).

[27] Waldman, S., Genet, G., Bastón, S., Side, J., 2015. Correcting for mesh size dependency in a regional model's representation of tidal turbines. In: Proceedings of the 11th European Wave and Tidal Energy Conference (EWTEC).

[28] Warren, I. R., Bach, H. K., 1992. MIKE 21: a modelling system for estuaries, coastal waters and seas. Environmental Software 7 (4), 229–240.

[29] Whelan, J. I., Graham, J. M. R., Peiro, J., 2009. A free-surface and blockage correction for tidal turbines. Journal of Fluid Mechanics 624, 281–291.

[30] Yang, Z., Wang, T., Copping, A. E., 2013. Modeling tidal stream energy extraction and its effects on transport processes in a tidal channel and bay

system using a three-dimensional coastal ocean model. Renewable Energy 50, 605–613.